A. F. Blom, A. Hedlund,† W. Zhao,‡ A. Fathulla,‖ B. Weiss,‖ and R. Stickler‖*

Short Fatigue Crack Growth Behaviour in Al 2024 and Al 7475

REFERENCE Blom, A. F., Hedlund, A., Zhao, W., Fathulla, A., Weiss, B. and Stickler, R., **Short Fatigue Crack Growth Behaviour in Al 2024 and Al 7475**, *The Behaviour of Short Fatigue Cracks*, EGF Pub. 1 (Edited by K. J. Miller and E. R. de los Rios) 1986, Mechanical Engineering Publications, London, pp. 37–66.

ABSTRACT The present investigation consisted of a study of fatigue crack initiation and growth in two high-strength technical Al alloys (Al 2024 and Al 7475) differing in mechanical properties and microstructure. Emphasis was on experiments at low load amplitudes slightly below and above the fatigue limit. Attempts were made to investigate the effect of stress ratios ($-1 \leq R \leq 0.7$) and to provide quantitative information on both the short crack and long crack growth behaviour for identical specimen material, orientation, and test conditions. To determine closure stresses a dynamic compliance technique was developed and the crack opening phenomena followed by microscopy methods. Initiation and growth of fatigue cracks were found to be strongly dependent on microstructural features (second phase particles, grain boundaries). A comparison of the growth behaviour of both microstructurally-short and physically-short cracks with that of long cracks shows that the peculiarities of short crack growth can be partly related to crack closure phenomena.

Introduction

Since the early observations by deLange (**1**) on the apparently anomalous growth of fatigue microcracks and the subsequent findings of Pearson (**2**) that fatigue cracks show the characteristic long crack growth behaviour only beyond a certain crack length, the phenomenon of short crack behaviour has attracted considerable interest. The magnitude of research efforts and the increasing number of pertinent publications reveal not only academic interest but also technical relevance and engineering consequences of the short crack problem (**3**)(**4**).

The state of knowledge on the behaviour of short fatigue cracks has been documented and reviewed in several publications (e.g., (**5**)–(**11**)) and in contributions to the Euromech colloquium 151 on the creation and behaviour of such cracks, e.g., (**12**).

In spite of the world-wide research effort, some aspects of short crack behaviour still appear ill understood (**13**). Information on initiation sites in pure metals and technical alloys is controversial (e.g., (**2**)(**5**)(**14**)–(**19**)). In contrast to long fatigue cracks (LC) there exists no adequate definition of the growth mechanisms, the crack tip stress/strain fields, or the interactions with

* The Aeronautical Research Institute of Sweden, Bromma, Sweden.
† The Royal Institute of Technology, Stockholm, Sweden.
‡ The Chinese Aeronautical Establishment, Beijing, People's Republic of China.
‖ University of Vienna, Austria.

microstructural features, for short fatigue cracks (SC). The specificities in SC growth have been associated with closure effects which vary with increasing crack length (**11**)(**15**)(**20**), and mechanisms which give rise to closure with increasing crack length have been proposed (**21**)–(**24**). Considerable attention was given to the interaction of SC with crystallographic features, the effects of microstructure (**12**)(**25**)(**26**)(**43**), and the effects of crack deflection at grain boundaries (**27**)–(**29**). Only a little information can be found about the effects of stress ratios on SC behaviour (**11**)(**25**). Investigations on SC growth in notches (**18**)(**19**)(**30**) indicate no difference to plain specimens as long as the tests are carried out at low stress amplitudes (negligible notch plasticity effects).

Many investigators found it convenient to present SC growth data in combinaton with LC data as a function of the stress intensity range, in spite of the fact that the applicability of the K concept to cracks smaller than a critical size was already questioned by Kitagawa (**38**). The breakdown of the similitude requirements of LEFM in the case of SCs was pointed out in several publications (e.g., (**3**)(**6**)(**8**)).

Various hypotheses have been proposed to quantify the transition from SC to LC behaviour (**9**)(**31**)–(**37**). Based on a diagrammatic presentation of log stress-range versus log crack-length first suggested by Kitagawa (**38**), three regions of growth behaviour can be differentiated, i.e.: (i) the SC region in which the presence of a SC does not affect the plain specimen fatigue limit; (ii) a transition region in which the threshold stress for fatigue crack growth is gradually lowered with increasing crack length (EPFM considerations); and (iii) the region in which the growth of a fatigue crack follows LEFM relations, i.e., the LC region. Several authors have employed such a type of presentation for a general description of SC behaviour, but, little quantitative information is available with respect to the extent of these three regions and, in particular, how variations in stress ratio influence the respective border lines (**39**). As indicated in Table 1, LC growth behaviour in Al alloys was reported by various authors to occur beyond a crack length of 100–300 μm. Recent experimental results (**16**)(**17**) indicate that the border between SC and LC behaviour can be defined uniquely by applying the value of the effective threshold stress intensity, assumed to be a material parameter which can be determined experimentally and should remain unaffected by the stress ratio.

A considerable amount of information regarding SC behaviour has been published for engineering high-strength Al alloys, as summarized in Table 1. It can be seen that most of these investigations were carried out at relatively high stress amplitudes approaching the yield strength of the alloys, and in general for only a relatively small number of loading cycles. Thus, experimental values listed for fatigue limits and threshold stress intensities may be higher than the true limiting values. A direct comparison of SC and LC behaviour is frequently lacking for the same material.

The present investigation consisted of a detailed study of fatigue crack initiation and growth in two high-strength technical Al alloys differing in

Table 1 Published information on short crack growth behaviour in Al alloys

Reference	*Alloy*	*Testing conditions*			*da/dN* m/c	*Method of SC observation*	*Remarks*
		$\sigma_u/\sigma_{0.2}$	R	*Frequency (Hz)*			
de Lange (**1**)	26ST	—	—	—	10^{-7}–10^{-5}	replica SEM	non-propagating cracks 5–10 grain diameters
Pearson (**2**)	DTD 5050 (~7075-T651) L65 (~2014-T3)	0.4–0.6	0.1 to 0.78	25	$>10^{-9}$	LM	LC > 127 μm
Morris (**15**)	2048-T851	0.6–0.9	−1	5	—	in situ SEM	observation of residual closure
Morris *et al.* (**21**)(**40**)(**41**)	2219-T851	0.7–0.9	−1	5	—	LM LM-stereo imaging	microcrack closure
Kung, Fine (**19**)	2024-T4, 2124-T4	0.65–1.16	−1	—	2×10^{-8}	in situ LM	crack tip plasticity LC > 300 μm
James *et al.* (**24**)(**26**)(**42**)	2219-T851 7075-T6	0.6–0.9	0, −1	5	$>10^{-9}$	—	LC > 5–15 grain diameters
Nisitani, Takao (**5**)	Al-alloy annealed	2.3	−1	50	—	—	
	Al-alloy hardened	0.6	−1	50	—	—	
Hirose, Fine (**30**)	PM-X 7091 (MA87)	0.3–0.8	−1	25	—	in situ, replica-SEM	initiation at grain boundaries
Lankford *et al.* (**29**)(**44**)–(**46**)	7075-T651, -OA, -T6, 6061-T6	0.8	0.1	1–5	$>2 \times 10^{-10}$	SEM-stereo imaging	Strain distribution, COD
Foth *et al.* (**18**)	2024-T3	(high)	0	—	$>2 \times 10^{-6}$	LM	influence of notches
Fathulla *et al.* (**16**)(**17**)	2024-T3	0.29–0.52	−1	20 000	5×10^{-13}– 5×10^{-11}	in situ LM replica-SEM	topography of short cracks transition length to LC between 220–250 μm significance of $\Delta K_{th,eff}$

mechanical properties and microstructure. Emphasis was put on performing the cyclic experiments at low load amplitudes slightly below and above the high-cycle fatigue limit or the threshold stress intensity. Attempts were made to investigate the effect of mean stress, and to provide quantitative information on SC and LC growth behaviour for identical specimen material, orientation, and test conditions. For the determination of closure stresses a dynamic compliance technique was developed and the crack opening phenomena followed by microscopy methods. Experimental data were compared to FEM calculations on the extent and shape of plastic zones at the tips or in the wake of short and long fatigue cracks.

Specimen materials and experimental techniques:

In a continuation of previously published studies on the long crack (LC) and short crack (SC) growth behaviour (**16**)(**17**) further measurements were carried out on the high-strength alloy Al 2024-T3. Specimens from the same lot were available for detailed investigations of the closure effect and the transition from SC to LC growth. In addition, specimens from a batch of the alloy Al 7475-T761 were selected for a comparative study. This alloy is known to exhibit higher strength, fracture toughness, and, in particular, higher stress corrosion cracking resistance than alloy Al-2024.

Composition, heat treatment, grain dimensions, and tensile properties of the specimen materials supplied in plate form (2 and 6 mm thickness) are listed in Table 2.

The thermomechanical pretreatment of the plate material resulted in a typical pancake-type grain structure. Both alloys were found to contain several phases, in agreement with published information (**47**) coarse particles were identified by EDAX analysis to correspond to the following intermetallic compounds.

Al 2024: insoluble coarse particles of $Al_{12}(Fe,Mn)_3Si$ and Al_7Cu_2Fe;
partially soluble Mg_2Si, Al_2Cu_2Mg;
and, in recrystallized material, $Al_{20}Cu_2Mg$.

Al 7475: insoluble coarse particles of Al_7Cu_2Fe;
partially soluble Mg_2Si, dispersoid of $Al_{12}Mg_2Cr$.

No attempts were made to investigate the nature and morphology of the hardening precipitates (i.e., Al_2Cu_2Mg in Al 2024 and $Mg(Al,Cu,Zn)_2$ in Al 7475 (**47**)).

Pertinent information on test procedures and specimen geometries for both alloys are summarized in Table 3 and are briefly discussed below.

(*i*) For the conventional S–N fatigue tests (using a 'LF' Schenck servo-hydraulic test system at $-1 \leq R \leq 0.75$, and 40–80 Hz, specimens with cylindrical gauge sections were machined from the plate material. However at low stress amplitudes (near the fatigue limit) experiments were performed on a

Table 2 Specimen materials and properties

Chemical composition (*weight %*) *Element*	*Al 2024* (*nominal*)	Al 7475 (*actual*)
Cu	4.5	1.8
Mg	1.5	2.3
Mn	0.6	0.5
Si	0	0.04
Zn	0	5.8
Cr	0	0.22
Fe	—	0.10
Ti	—	0.003
Al balance	balance	balance
Heat treatment	*Al 2024*	*Al 7475*
Commercial	T3	T761
Grain size (*mean intercept method*) (*μm*)		
Alloy	*Al 2024*	*Al 7475*
Plate thickness (mm)	6	2 6
Orientation:		
longitudinal, L	120	150 350
Transverse, T	65	80 150
Short transverse, ST	25	20 20
Tensile properties		
Alloy	*Al 2024*	*Al 7475*
Plate thickness (mm)	6	2 6
Orientation	L	L T L T
$\sigma_{0.2}$ (MPa)	345	463 449 482 475
σ_{UTS} (MPa)	450	510 514 526 543
A (%)		14 15 15 12
HV		161 170
Dynamic Young's Modulus (GPa)	72.5	70.5 71.4

'HF' resonance system ($R = -1$, test frequency 20 kHz) (**48**). HF-SN data were obtained with specimens of either a cylindrical gauge section or with specimens of a rectangular cross section containing a mild notch. In the latter case the stress amplitudes listed in Table 3 correspond to the surface stress in the root of the notch, determined experimentally with miniature strain gauges. These values were found to be in good agreement with values calculated by a stress concentration factor computed for this notch geometry by finite element methods; see Fig. 1.

(*ii*) The long-crack (LC) growth behaviour was studied at LF frequencies with standard compact-tension (CT) and centre-notched (CN) specimens. Fatigue crack growth data were determined in accordance with the proposed

Table 3 Test methods and specimen geometries

Test method	*Stress ratio*	*Specimen geometry (plate thickness)*	*Specimen orientation*	
			Specimen axis	*Crack growth direction*
S–N *data (endurance limit)**				
LF, $N_{max} = 1 \times 10^7$	$-1 < R < 0.75$	cylindrical (6 mm)	L	T
HF, $N_{max} = 2 \times 10^8$	$R = -1$	cylindrical (6 mm)	L	T
		(gauge section 4 mm diam.)	T	L
LC growth data (da/dN–ΔK, ΔK_{th}, $\Delta K_{th,eff}$)†				
LF	$-1 < R < 0.75$	CT,CN (6 mm)	L	T
			T	L
HF	$R = -1$	CN (6 mm)	L	T
			T	L
SC growth data (c–N, dc/dN–c)				
LF	$R = 0.05$	side notch (2 mm)	L	ST
HF	$R = -1$	side notch (6 mm)	L	ST

L rolling direction
T transverse directon
ST short transverse direction
* Al 7475 tested only at $R = 0.05$.
† Al 2024 tested only with stress axis in the L direction.

ASTM standard procedure (**49**)(**50**). For the HF tests CN specimens were used, containing either a through-thickness starting notch or a lancet-shaped surface notch giving rise to semi-elliptical crack growth (ASTM Standard Practice E740-80 (**51**). Threshold values corresponding to fatigue crack growth rates of less than 1×10^{-13} m/cycle were obtained by a strain shedding technique (**52**). The computational procedure developed for the HF tests have been reported for through-thickness cracks (**50**) and for semi-elliptical surface cracks (**52**). Following ASTM recommendations, only the tensile part of the stress cycle at negative R values was taken for the calculation of ΔK_{th}.

(*iii*) The crack closure stress (defined here as the first contact of crack surfaces at diminishing cyclic amplitudes) and the effective threshold stress intensity values were determined by the test procedure described in reference (**50**).

(*iv*) The SC growth behaviour was studied with full-thickness plate specimens of rectangular cross-section. Cylindrical side notches were machined into one of the narrow sides of the specimens in order to reduce the surface area to be scanned during cyclic loading. To calculate the surface stresses in the notch root

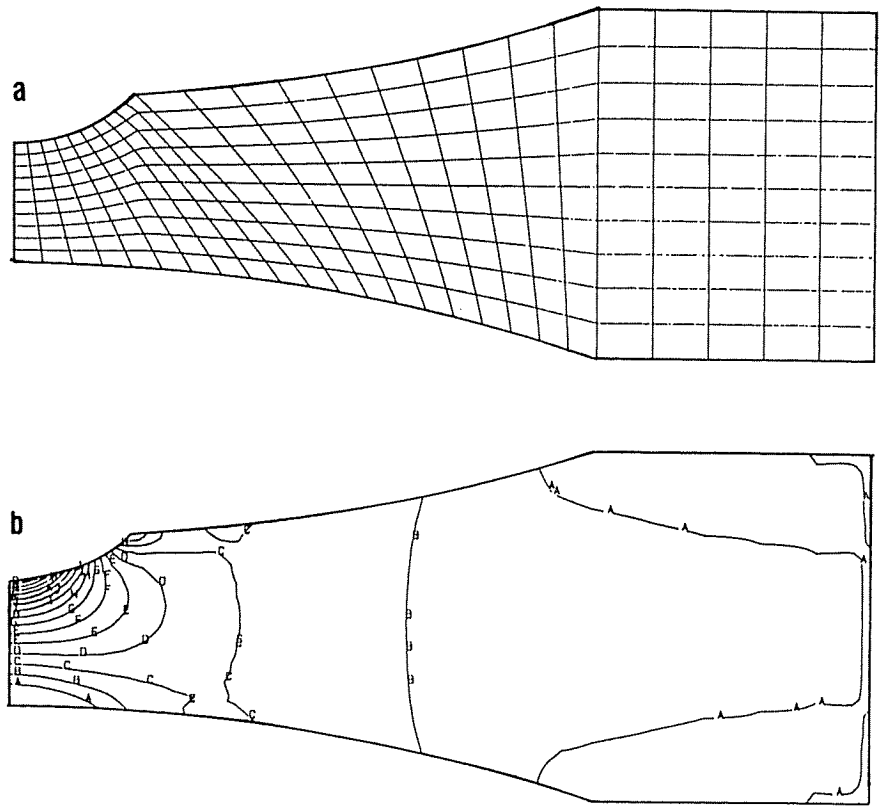

Fig 1 Stress determination of a side-notched specimen with $K_t = 2.468$
(a) Finite element discretization
(b) An isostress plot

we used stress concentration factors computed by FEM. The selected notch geometries resulted in nominal K_t values between 1.1 and 2.97. For the low stress amplitudes applied in these tests (maximum surface stress always smaller than the yield strength) it was assumed that effects of notch-root plasticity can be neglected.

To observe the initiation and to follow the growth behaviour of short fatigue cracks under LF test conditions a SEM-replica method was applied. Plastic replicas were prepared of the specimen surface after appropriate numbers of loading cycles and micrographs recorded of corresponding surface areas. During the HF tests the specimen surface could be directly examined at high resolution under a light microscope. This is possible because of the fact that, for specimens excited to resonance vibrations at the lowest 'eigen' frequency, the maximum in strain amplitude in the mid-section of the specimen coincides

with the location of zero displacement. The microscopic observations were continuously recorded on video-tape (synchronously with pertinent experimental data) to permit a post-test quantitative evaluation. The SC growth measurements were extended to more than 10^7 loading cycles for each applied stress level. In this way information on retardation or halting of the crack growth, and on the interaction of the advancing crack with microstructural features could be collected with high sensitivity.

Experimental results

S–N data

Fatigue life curves determined by HF tests for both alloys at $R = -1$ are shown in Fig. 2. The data points obtained by LF testing fall within the respective

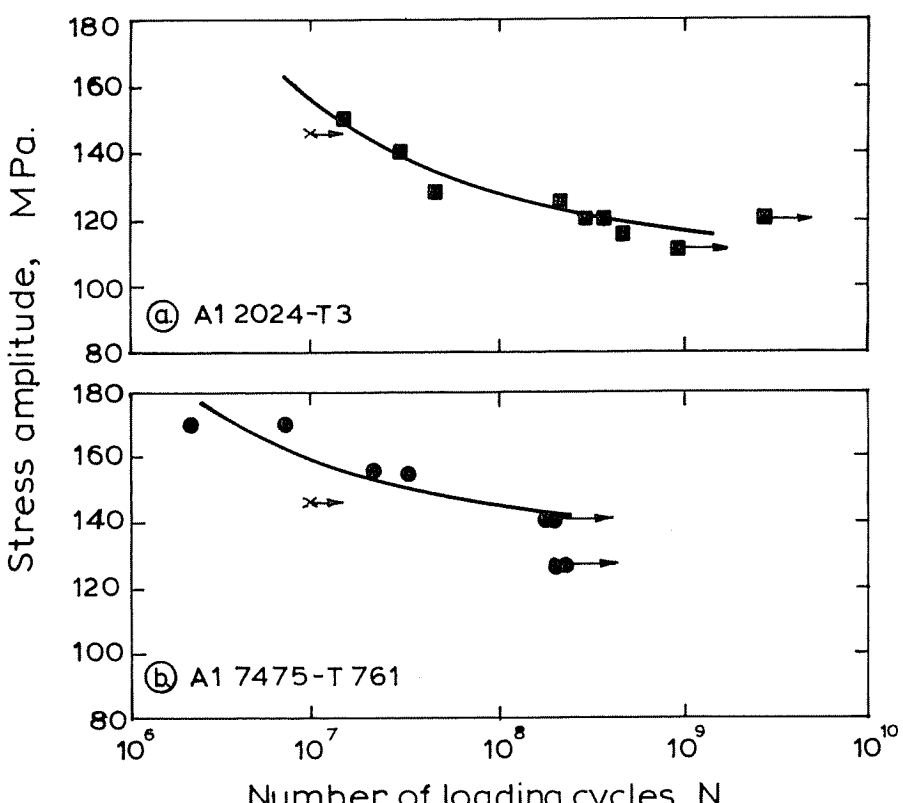

Fig 2 S–N data at $R = -1$ and room temperature, test frequency 20 kHz. Crosses indicate unbroken specimen tested at 50 Hz. Stress axis parallel to L direction

Table 4 Effect of stress ratio on fatigue strength of Al 2024 and Al 7475

Alloy	*Al 2024*		*Al 7475*	
Test method	*LF*	*HF*	*LF*	*HF*
N_{max}	1×10^7	2×10^8	1×10^7	2×10^8
Endurance limit (MPa) at:				
$R = -1$	147	128	142*	148
$R = 0.05$	117		115	
$R = 0.5$	76		80*	
$R = 0.75$	45		45*	

* Taken from literature.

scatterbands, indicating the absence of a pronounced frequency effect on fatigue life. Microscopy examination of the specimen surface in the gauge section of unfailed specimens revealed the presence of non-propagating microcracks. The S–N curves reveal that a true fatigue limit may not exist or may not be reached prior to 10^8 loading cycles.

An extensive investigation of the effects of test frequency in the applied frequency range (**53**)(**54**) has shown that, for ductile fcc materials, a small frequency effect on the fatigue limit and the threshold stress intensity of long cracks can be attributed mainly to thermally activated processes. For high-strength materials the frequency effect in the near-threshold regime can be considered as practically negligible (**50**).

The effect of the stress ratio R on fatigue life of Al 2024 and Al 7475 can be deduced from the values listed in Table 4.

Long crack growth and threshold behaviour

Fatigue crack growth curves for Al 2024 tested at various R values have been published previously (**50**). The FCG behaviour of Al 2024 and Al 7475 is shown in Fig. 3.

The effect of stress ratio, specimen orientation, and test frequency on the LC threshold stress intensity of both alloys can be deduced from Fig. 4. It can be seen that for the same orientation the threshold values of the stronger Al 7475 fall below that of Al 2024 over the whole range of R.

This difference is also apparent in the values of the effective threshold stress intensity plotted for both alloys in the same diagrams. It should be noted, however, that the values of ΔK_{th} and $\Delta K_{th,eff}$ could only be determined with an accuracy not better than 10 per cent.

Metallographic observations do not show any resolvable plastic zones associated with the crack advancing near threshold in both alloys. In Al 7475 a tendency to localized decohesion along glide planes (resulting from the preceding cold work) can be recognized. An evaluation of the fracture topography,

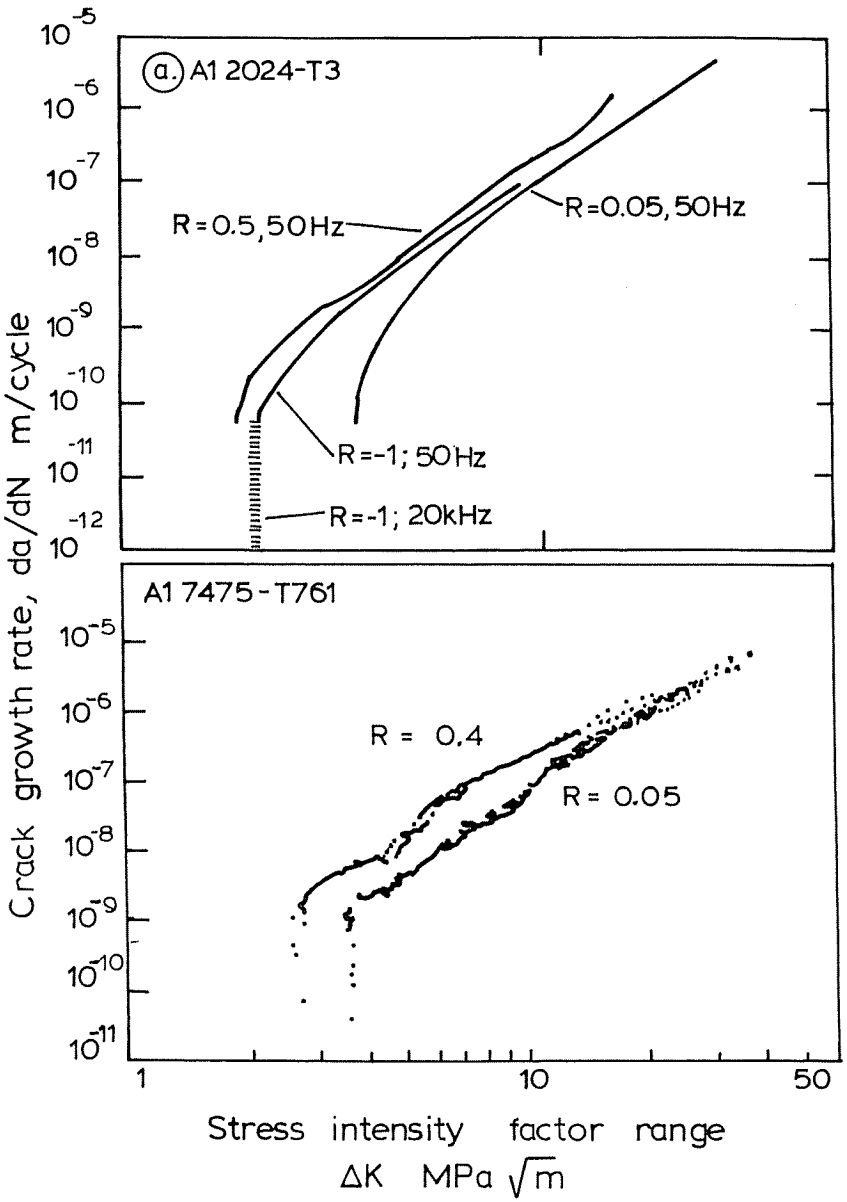

Fig 3 Fatigue crack growth data for various stress ratios and test frequencies determined at room temperature. The crack plane in Al 7475 is parallel to the L direction

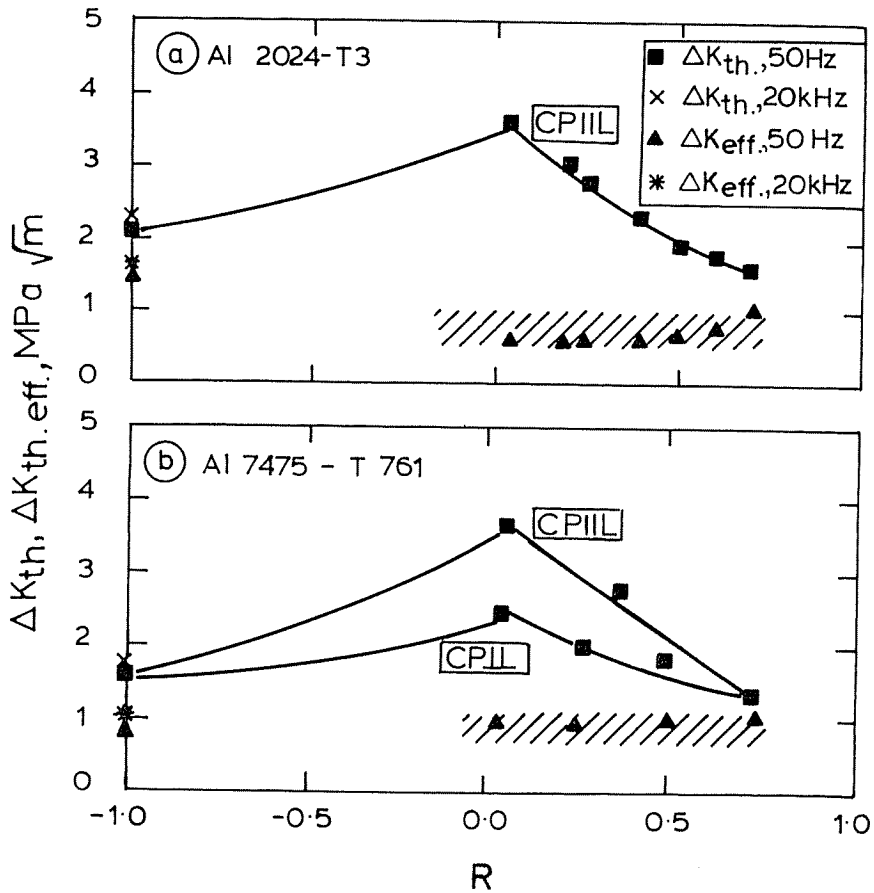

Fig 4 Effect of stress ratio, specimen orientation, and test frequency on threshold stress intensity and effective threshold stress intensity

however, reveals a difference in the crack path irregularity between the two alloys. This irregularity can be expressed by a roughness parameter (55), i.e., the ratio of the actual length of the crack at the specimen surface and the length of the crack projected onto a straight line normal to the stress direction, l_{act}/l_{proj}. This roughness parameter was determined for Al 2024 as 1.15 and for Al 7475 as 1.05. Thus, the differences between threshold and effective threshold values in Al 2024 and Al 7475 appear mainly to be due to various degrees of geometrically induced closure, with oxide induced closure a possible contributory factor.

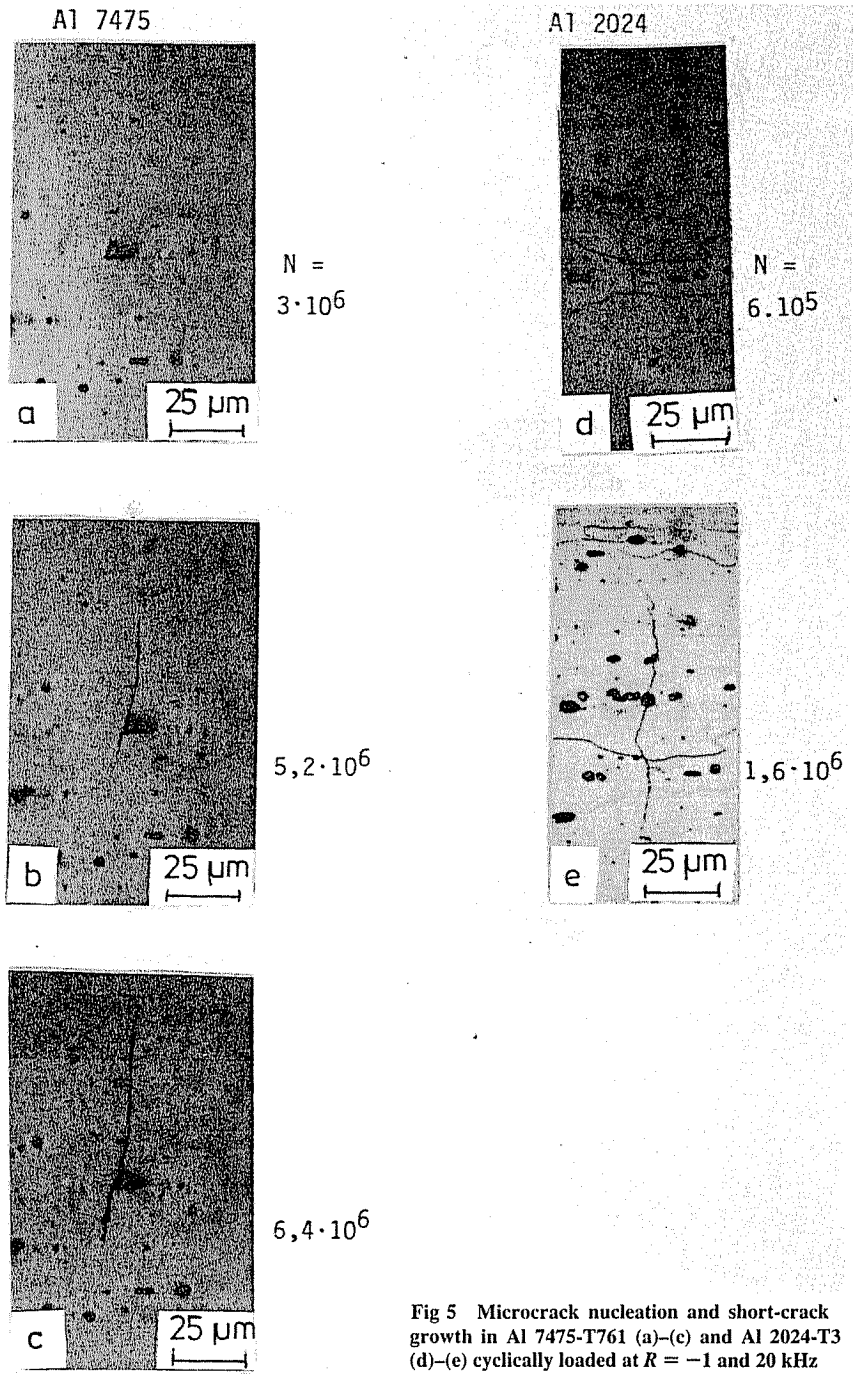

Fig 5 Microcrack nucleation and short-crack growth in Al 7475-T761 (a)–(c) and Al 2024-T3 (d)–(e) cyclically loaded at $R = -1$ and 20 kHz

Short crack initiation and growth

Microscopy observations during $R = -1$ fatigue loading (see Fig. 5), revealed that crack nucleation occurs in Al 2024 at fractured bulky (Fe,Si containing) intermetallic particles, the fracturing taking place during fatigue. In Al 7475 crack nucleation proceeded occasionally along a particle/matrix interface, but also inside a grain and apparently related to a slip band. Cracking of intermetallic particles during fatigue loading was not observed in Al 7475.

The growth of such microcracks in Al 2024 is represented in the c–N and dc/dN–c curves of Fig. 6. Here c represents the half-length of the surface crack which was assumed to be semi-elliptical. The penetration, a, of these surface cracks, was determined by fractographic evaluation of specimens ruptured after completion of the short-crack measurements. A shape factor a/c decreasing from 0.9 to 0.6 for fatigue cracks increasing from $c = 20$ to $c = 300$ μm was found for Al 2024. The *np* line of Fig. 6(a) represents an initially non-propagat-

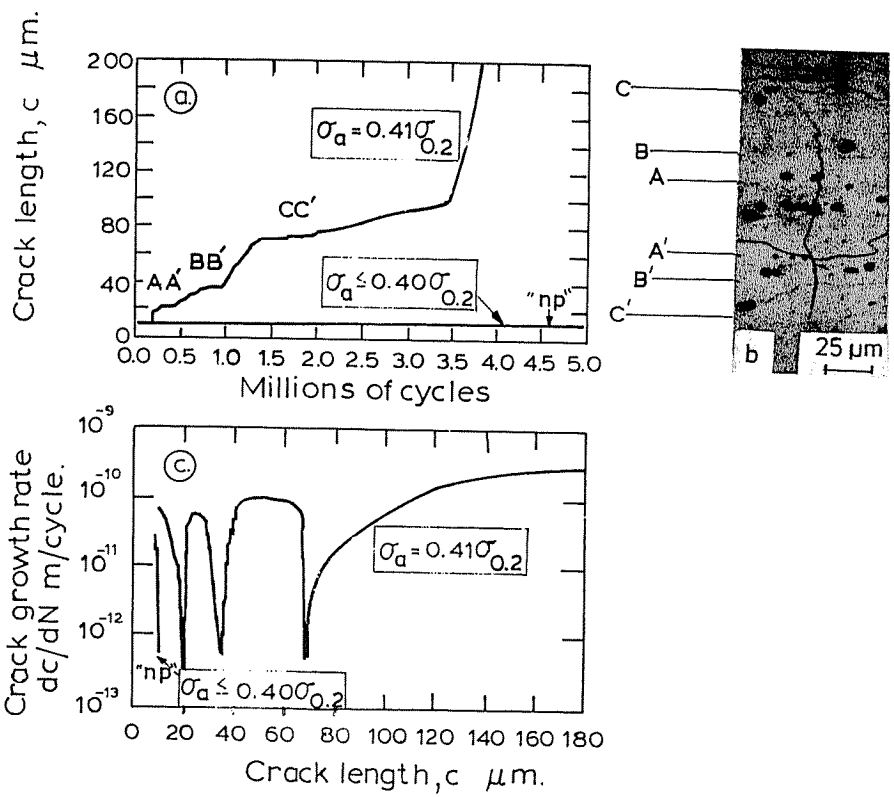

Fig 6 Growth behaviour of short cracks in Al 2024-T3 during cyclic loading at $R = -1$ and 20 kHz. Crack plane parallel to ST

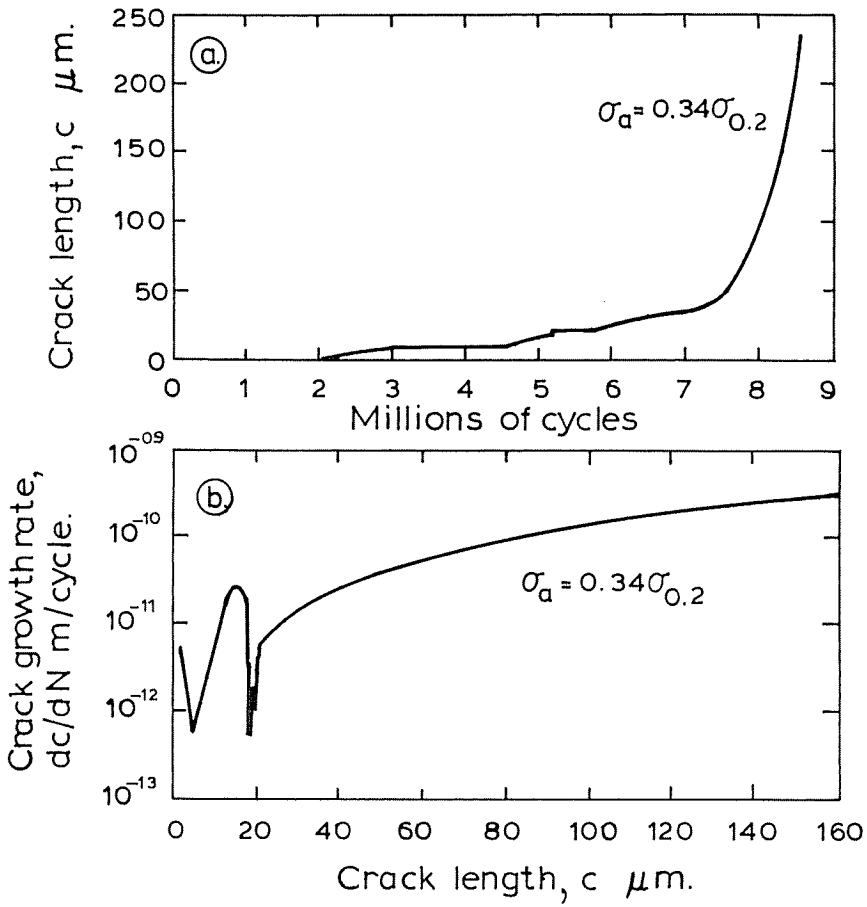

Fig 7 Growth behaviour of short cracks in Al 7475-T761 during cyclic loading at $R = -1$ and 20 kHz. Crack plane parallel to ST

ing microcrack which continued growth after a slight increase in stress amplitude (interacting with microstructural features such as grain boundaries) up to a length of 110 μm as shown in the micrograph, Fig. 6(b).

Similar curves for Al 7475 at $R = -1$ are shown in Fig. 7 and for $R = 0.05$ in Fig. 8 for two different stress levels. These stress levels correspond to crack initiation after 10^4 and 10^5 loading cycles, respectively, and thus fall above the HF *S–N* curve. The equivalent stress levels for the tests at $R = -1$ are only slightly larger than the fatigue limit at $N = 5 \times 10^8$ of the corresponding *S–N* curve. An evaluation of the effect of stress levels on the short crack growth behaviour must take into account that the *S–N* curve for $R = -1$ is above that

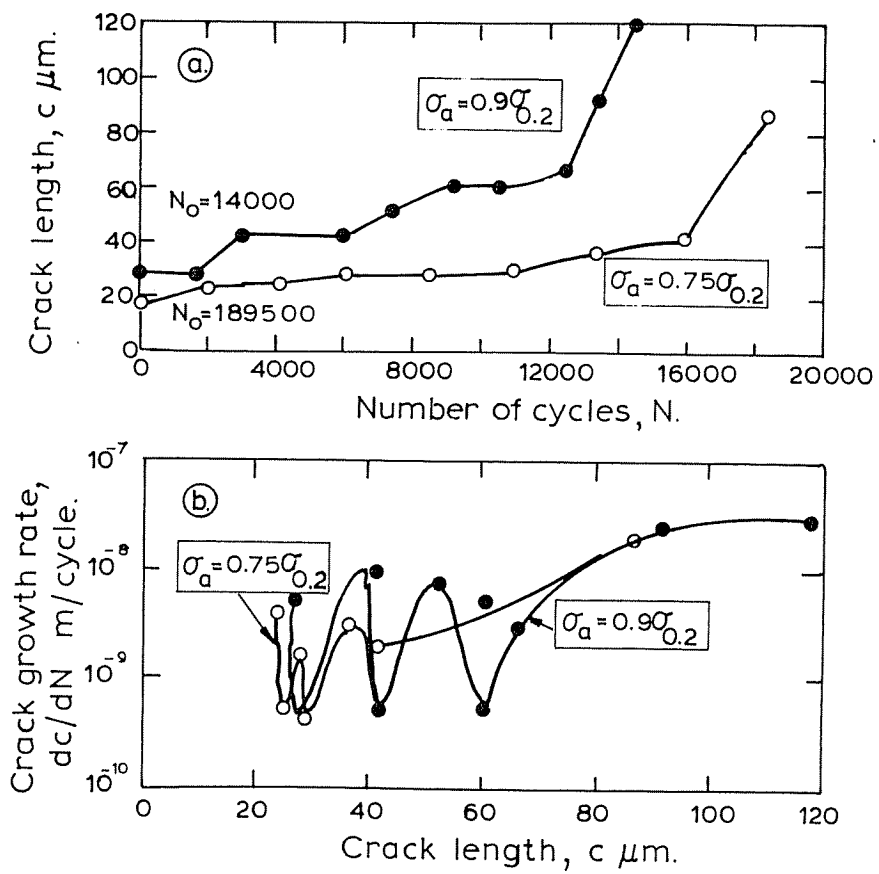

Fig 8 Growth behaviour of short cracks in Al 7475-T761 during cyclic loading at $R = 0.05$ and 50 Hz for two stress amplitudes. Crack plane parallel to ST

for $R = 0.05$. A non-uniform crack tip advance can be recognized up to a characteristic crack length which is considerably shorter for Al 7475 as compared to Al 2024. Beyond this length the cracks appear to advance uninhibited. The microscopic observations indicate that the advance of both tips of a crack at the specimen surface does not always occur at equal rates.

Crack growth rates deduced from the above *c–N* curves are also plotted as function of crack length for Al 7475 in Figs 7 and 8. The higher cyclic stress levels in the $R = 0.05$ tests result in faster crack growth rates than in the case of $R = -1$. Retardation of the crack advance occurred when a crack tip approached a grain boundary. The degree of this retardation can be deduced from the numbers of loading cycles required to initiate a resumption of crack growth in the next grain. In the case of the low-amplitude HF tests at $R = -1$

retardation was observed to extend up to more than 10^6 cycles, while in the LF tests at $R = 0.05$ at the higher cyclic amplitudes the grain boundary retardation amounted typically only to 10^3 cycles. Consequently, the minima in the respective LF growth-rate curves are less pronounced, with intermittent maxima somewhat higher due to the higher stress amplitude.

A cessation of the interaction of the advancing crack with microstructural features (predominantly grain boundaries) can be recognized in the dc/dN curves at characteristic values of crack length, depending on stress amplitude and stress ratio.

Topographical features of short fatigue cracks

Optical and electron microscopy observations revealed typical features of the crack path which appear to characterize short crack behaviour and the transition from short crack to long crack growth. A clear transition in the crack advance from Stage I (transcrystalline crystallographic) to Stage II (trans crystalline non-crystallographic) with an intermediate transition region (localized crystallographic Stage II) for Al 2024 could also be deduced from the micrographs for Al 7475; Fig. 9. For Al 2024 this transition was found to

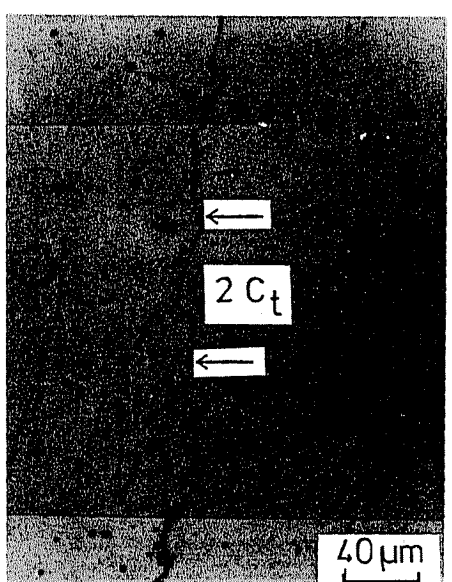

Fig 9 Micrograph of a short crack in Al 7475–T761 after cycling at $R = -1$ and 20 kHz at a stress level of $\sigma_a = 0.34\sigma_{0.2}$. The transition length $2c_T$ is indicated by arrows and marks the change from transcrystalline Stage I to crystallographic Stage II crack propagation

Table 5 Characteristic crack lengths for transition from short-crack to long-crack growth behaviour

Alloy	R	*Stress amplitude (MPa)*	N_{max}	ΔK_{th} ($MPa\,m^{1/2}$)	$\Delta K_{th,eff}$ ($MPa\,m^{1/2}$)	c_{eff} (μm)	c_T (μm)	c_2 (μm)	c_1 (μm)
Al 2024	−1	128	5×10^8	2.15	1.3	90	110	140	400
Al 7475	−1	148	2×10^8	1.62	0.9	30	45	—	—
	0.05	356	1.8×10^5	—	—	—	40	—	—

correspond to a characteristic crack length, apparently not related to the grain dimensions (**17**). The measured transition length c_T for alloys Al 2024 and 7475 are listed in Table 5. It is interesting to note that this characteristic transition length compares reasonably well with the critical crack length indicated in the dc/dN–c curves from constant amplitude fatigue tests at which the marked retarding effect of grain boundaries ceases.

Discussion

Transition from short-crack to long-crack growth

Pertinent test results for Al 2024 are summarized in the Kitagawa-type diagram of Fig. 10. It can be seen that the sloping line computed for ΔK_{th} of a semi-elliptical crack intersects the horizontal line corresponding to the fatigue limit ($N = 5 \times 10^8$) at a crack length, termed c_0 in the literature, of approximately 240 μm. As will be shown in the following this mathematical value appears to have little physical meaning. Comparable results were also found for through-thickness cracks.

If we assume that the horizontal line resembles the true fatigue limit we may surmise the absence of propagating SCs below this line. Indeed, metallographic observations failed to reveal even non-propagating microcracks below this stress level. Above this stress level microcracks were observed which exhibited characteristic SC behaviour (crystallographic transcrystalline through entire grains) in the stress range up to approximately 1.5 times the fatigue limit.

As described earlier (**16**)(**17**) the threshold behaviour of such SCs was investigated by the following test sequence. A specimen was loaded at consecutively increasing amplitudes until crack nucleation and slow short crack growth to a crack length by 80 μm had occurred. Then the amplitude was lowered to approximately half of the fatigue limit, at which no further crack growth could be detected. A step-wise increase in loading amplitudes after each 10^7 cycles was repeated until a resumption of crack growth became noticeable; the corresponding stress amplitude was recorded as the threshold for growth of this particular SC. The test sequence was repeated for the same crack at incremental length values. The results are indicated in Fig. 10(a) by data points. It is

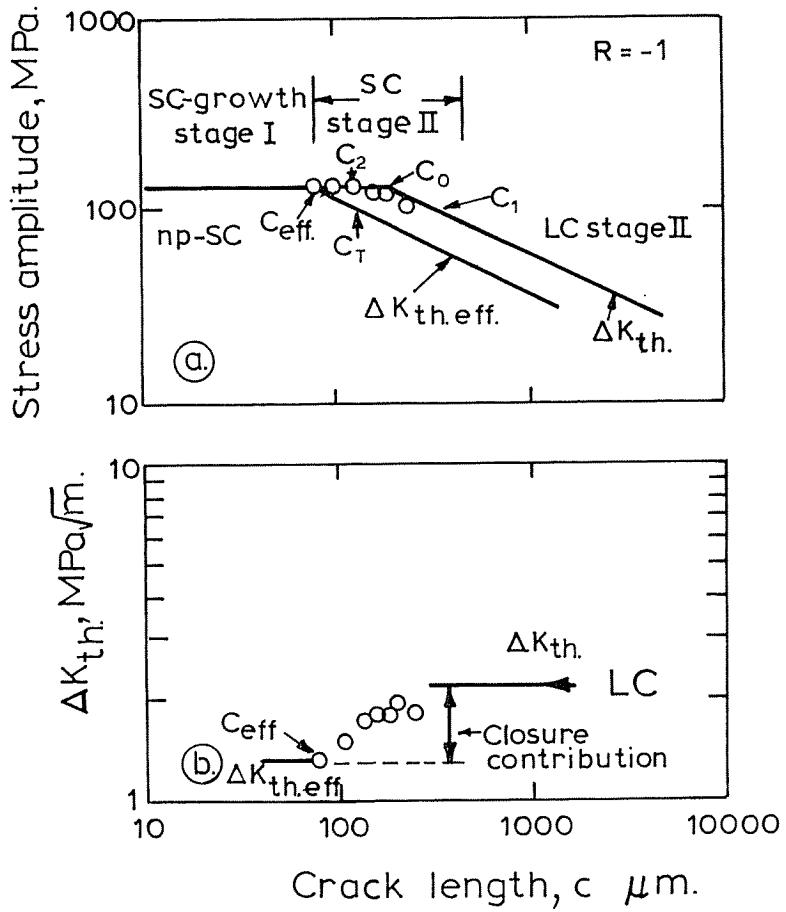

Fig 10 Summary of observations on crack growth behaviour in Al 2024-T3

(a) A Kitagawa stress-amplitude versus crack-length diagram. Data points indicate stress amplitudes for resumption of growth of the same 'short crack' at successively increasing lengths

(b) Apparent threshold stress intensities for the 'short crack' data points shown in Fig. 10(a)

interesting to note that resumption of crack growth occurred initially independently of crack length just above the fatigue limit. Beyond a crack length of approximately 140 μm (c_2 in Fig. 10(a)), a reduction in threshold stress became apparent. An extrapolation of the curve interconnecting these data points showed that the ΔK_{th} line is approached at a crack length of approximately 400 μm, that is, c_1 in Fig. 10(a). For cracks longer than this value the growth behaviour should obey conventional LEFM criteria.

The results show that SC growth below the fatigue limit takes place only in the narrow field between c_2 and c_1. Otherwise, SC growth behaviour (Stage I) prevailed in a small range above the fatigue limit, but only slightly to the right of the ΔK_{th} line, at which crack propagation changed to crystallographic Stage II. Longer cracks proceeded by the non-crystallographic Stage II mode.

Short crack growth and effective threshold stress intensity

Presuming the absence of closure effects for SCs it appears plausible that the SC growth behaviour ceases at a crack length corresponding to the intersection of the sloping line calculated for the experimental value of $\Delta K_{th,eff}$ and the fatigue limit line, as shown by c_{eff} in Fig. 10(a). We propose that the LEFM crack growth laws can be applied to cracks longer than c_{eff}, provided $\Delta K_{th,eff}$ is used instead of ΔK_{th}

Replotting the threshold stress intensity values as a function of crack length one finds a fall-off from the LC–ΔK_{th} at a crack length corresponding to c_1 along a line intersecting the $\Delta K_{th,eff}$ level at the crack length of c_{eff} = 90 μm (Fig. 10(b)). It should be pointed out, however, that the ΔK_{th} calculations have been carried out using an experimentally determined shape factor for cracks decreasing from c_1 to c_{eff}.

A further indication for a transition from SC to LC growth is apparent from the metallographic observations of crack path topography. As described above, crystallographic crack growth across entire grain diameters (at approximately 45 degrees to the stress axis, Stage I) changes with increasing length first to crystallographic Stage II (along segments of crystallographic planes zigzagging along a plane normal to the stress direction) and finally to conventional Stage II (non-crystallographic transcrystalline, essentially normal to the stress direction). The transition from Stage I to Stage II was found to be associated with a characteristic crack length, c_T = 110 μm. This transition length should again be related to the minimum length beyond which LEFM relationships may be applied to characterize crack growth.

A comparison of the crack growth behaviour, dc/dN, with the calculated ΔK_{th} values as a function of crack length, Fig. 11, shows clearly the relationship between cessation of anomalous short-crack growth (retarding effect of grain boundaries) at a crack length slightly larger than c_{eff}. Up to a crack length c_{eff} characteristic short crack growth occurs, indicating reduced effect of closure. Between c_{eff} and c_1 transition to long crack behaviour takes place. A summary of data on critical crack lengths is included in Table 5. The differences between c_{eff}, c_T, and c_2 may be due to the differing degrees of sensitivity of the respective test methods and actually may correspond to one and the same characteristic crack dimension. Moreover, part of the inconsistencies may be due to the fact that all the test results cannot be obtained from the same specimen, although all tests were carried out with specimens of the same orientation.

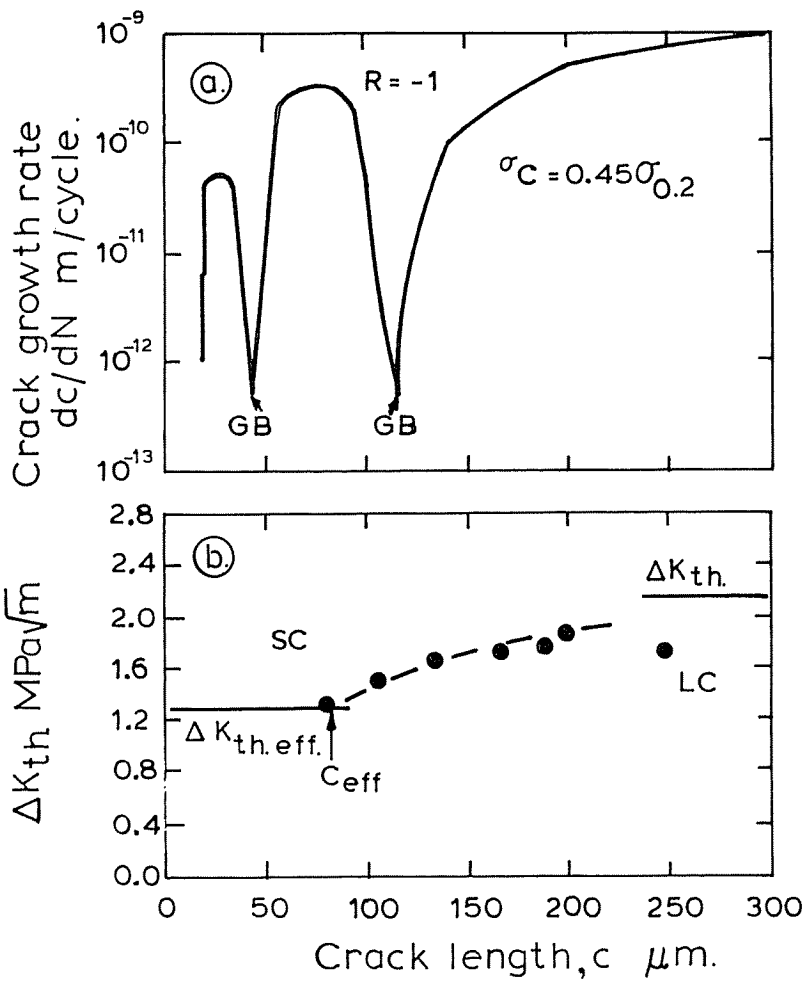

Fig 11 Relation between growth behaviour and threshold stress intensity values of a 'short crack' with successively increasing length in Al 2024-T3

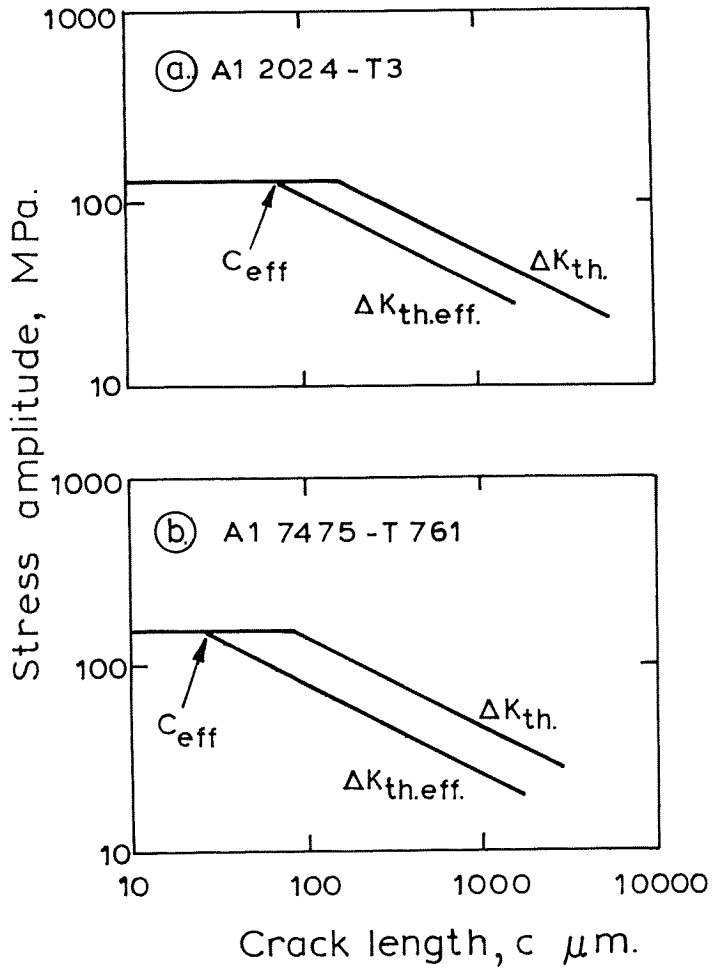

Fig 12 Comparison of crack growth behaviour in the two alloys. Note the significantly smaller value for c_{eff} in Al 7475

The test result for both alloys are compared in Fig. 12, which shows that the value of c_{eff} for Al 7475 is considerably smaller than for Al 2024, providing an explanation for the experimental difficulties encountered in monitoring SC growth behaviour in Al 7475.

To reveal the influence of the stress ratio on SC behaviour an attempt was made to plot the experimental results for the range of $-1 \leq R \leq 0.75$ in a Kitagawa-type diagram. Following a procedure employed by Usami and Shida (**39**) the LF data for Al 2024 are presented schematically in Fig. 13 in a modified maximum-stress versus crack size diagram. The sloping lines were calculated according to the relation

$$\Delta K_{th}/(1-R) = K_{th,max} = \sigma_{max} \cdot F(c^{1/2})$$

(where F is the geometry function) while the horizontal lines represent the fatigue limit as a function of the maximum stress (alternating stress plus mean

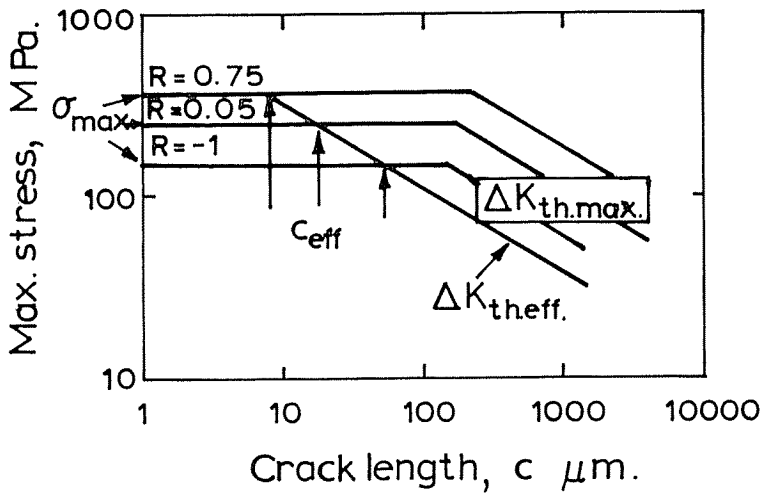

Fig 13 Semi-schematic presentation of the effect of stress ratio in Al 2024-T3

stress). It is interesting to note that in this presentation the intersection of both sets of lines occurs almost independent of the R value at a comparable crack length, c_o.

Under the assumption that the effective threshold stress intensity, $\Delta K_{th,eff}$, corresponds to the range between zero (at crack opening) and the maximum stress intensity actually encountered at the crack tip, $K_{th,eff,max}$, the sloping 'effective' line can be plotted according to the relation

$$K_{th,eff,max} = \sigma_{eff,max} \cdot F(c^{1/2})$$

The intersection of this 'effective' line (which corresponds to the whole range of R values) with the respective fatigue limits gives then the values of the critical crack length, c_{eff}, which resemble the border between SC and LC growth behaviour.

Non-closure of short cracks

Although at the present crack closure stresses cannot be measured with sufficient accuracy for cracks shorter than 500 μm, an indication of the closure effect can be obtained from the onset of a residual crack opening under zero load. As shown in the micrographs of surface replicas prepared at successive growth intervals of a particular short crack in Al 7475 (Fig. 14), lobes on the replicas associated with portions of the microcrack can be taken as an indication of non-closure of the mating fracture surfaces. The length of the cracks at which such lobes can be recognized first in the replicas is just slightly shorter than the measured transition length, $2c_T$.

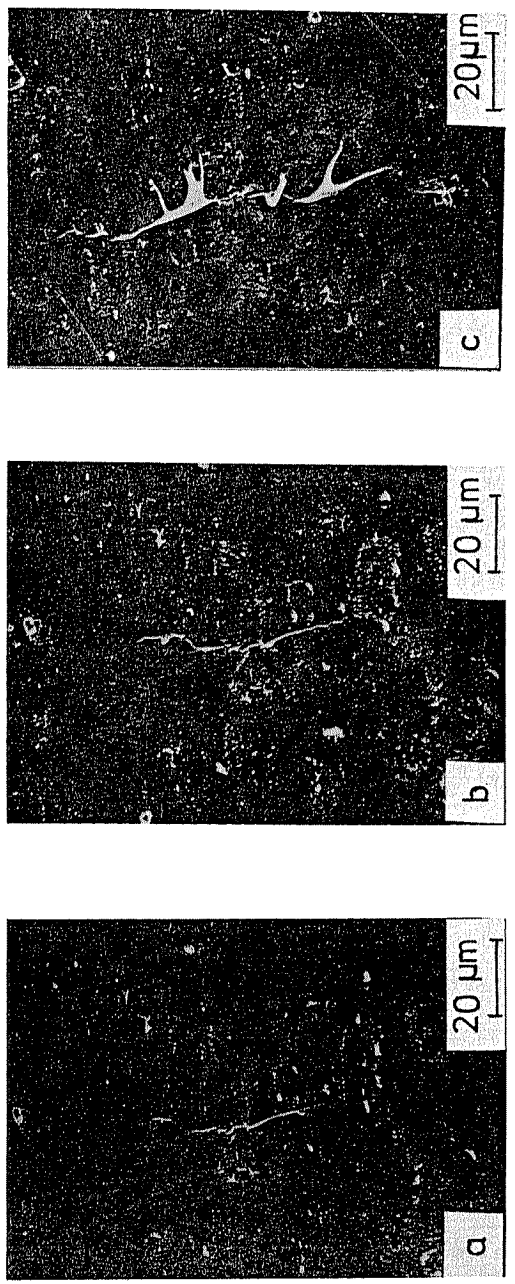

Fig 14 Scanning electron micrographs of surface replicas showing the development of residual crack opening with increasing length of a short crack in Al 7475-T761 cyclically loaded at $R = 0.05$ and 50 Hz and at a stress amplitude of $\sigma_a = 0.9\sigma_{0.2}$
(a) $N = 20\,000$ cycles
(b) $N = 23\,000$ cycles
(c) $N = 26\,500$ cycles

For a comparison of our test results on crack opening phenomena with data published by Lankford (**45**) one should take into account that Lankford's experiments were carried out at much higher stress levels, thus giving a considerably increased notch tip plasticity than in the case of our low-stress loading.

Plastic zones associated with short cracks

As discussed above there is experimental evidence for a characteristic transition length, c_{eff}, from microstructurally short cracks to elasto-plastic short cracks, and another characteristic transition length, c_1, to long cracks obeying a conventional LEFM growth relationship. The development of closure between c_{eff} and c_1 is expected to include not only plasticity-induced closure but also roughness-induced closure. In some cases, depending on material and environmental combinations, oxide induced closure may also be a contributing factor.

To verify, at least qualitatively, such closure development, and to obtain another estimate of the length c_{eff}, we shall consider in the following the pure plasticity effects of short, as compared to long, cracks. The results to be discussed are valid for Al 2024-T3 and are described in detail in (**56**). The calculations were carried out for a three-point bend specimen under a state of plane strain (which is supposed to be prevalent at the growth rates applied in the present investigation) and subjected to a constant cyclic load with a stress ratio of $R = 0$.

The numerical procedure described earlier (**32**) consists of elastic–plastic finite element calculations taking into account the propagation of a crack by releasing the crack tip node, changing the boundary conditions, and solving the contact problem occurring at the crack surfaces. In the computer program an initial isotropic strain hardening was assumed; the finite elements were two-dimensional triangles with cubic base functions. The initial crack length was taken as 10 μm and the size of the crack tip element was chosen to be 1.25 μm. Since the mesh in the vicinity of the crack tip was fine, it was expected that the correct crack tip singularity would be obtained.

In Fig. 15 some of the computed results of plastic zone sizes and shapes are shown. In Fig. 15(a) the plastic zone is shown for a very short crack of 10 μm length subjected to a nominal stress intensity range of $\Delta K = 2.31$ MPa$\sqrt{\text{m}}$. These results should be compared to results for a long crack with a length equal to one half of the specimen width and subjected to approximately the same driving force as for the short crack, $\Delta K = 2.56$ MPa$\sqrt{\text{m}}$, as shown in Fig. 15(b). We find that the local plastic flow is much easier in the case of the short crack than for the long crack, probably attributable to a reduced plastic constraint. It is also interesting to note the entirely different shapes of the plastic zones of short and long cracks. To produce approximately the same extent of the plastic zone as for the short crack at $\Delta K = 2.31$ MPa$\sqrt{\text{m}}$, a nominal driving force of $\Delta K = 6.4$ MPa$\sqrt{\text{m}}$ has to be applied to the long crack, Fig. 15(c).

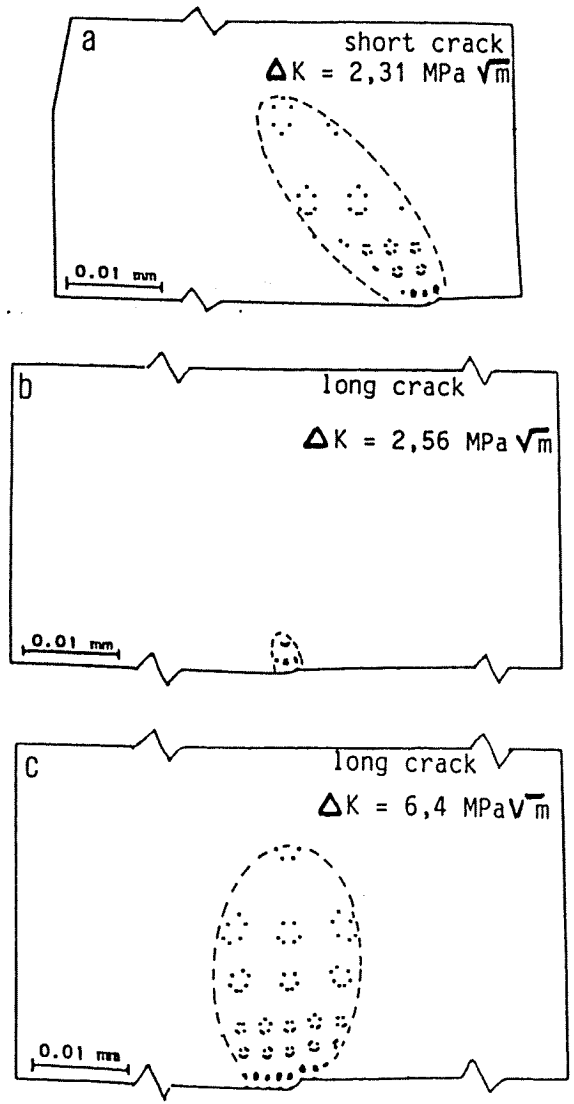

Fig 15 Shape and extent of plastic zones associated with the tips of short and long fatigue cracks from FEM computations

All the nominal stress intensity ranges mentioned above were calculated from the elastic displacement field by LEFM techniques.

As shown in Fig. 15(a), the plastic zone is formed in the direction of the maximum octahedral shear stress ahead of the crack tip, whereas no plasticity is contained in the wake of the short crack. This may indicate that the crack

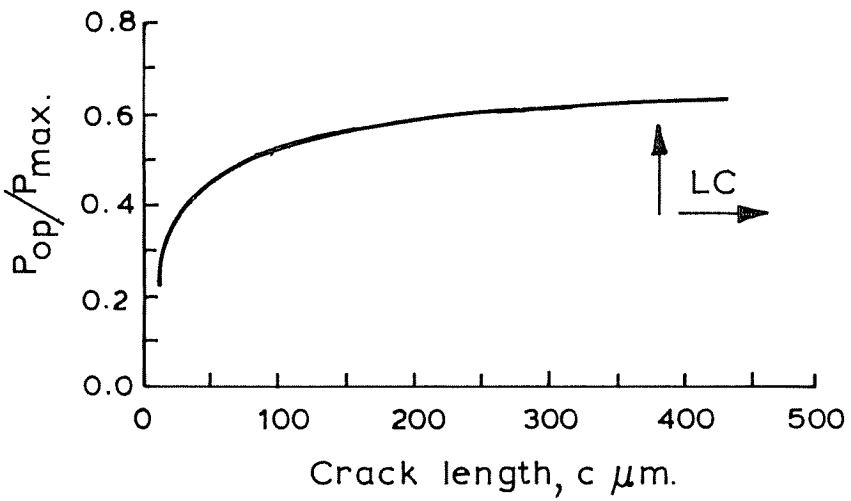

Fig 16 Development of crack closure (P_{op}/P_{max}) with increasing crack length. Results of FEM computations

favours a continued growth in slip planes oriented in this direction, a fact which is corroborated by experimental observations. If, instead, we consider the case of the long crack, we may predict that the crack would favour a conventional Stage II growth and that extensive plasticity would be left in the wake of the propagating crack. This in turn would cause plasticity-induced closure.

By performing a series of calculations with growing cracks (**56**) it could be shown that the development of crack closure can be calculated and plotted in terms of the load ratio P_{op}/P_{max}, as shown in Fig. 16. We find that the development of crack closure occurs rapidly for short cracks with increasing crack length, and that the saturation level for steady state behaviour occurs at a crack length of 400 μm. This value is in excellent agreement with our experimental result of c_1 for Al 2024-T3, as discussed above. The development of crack closure shown in Fig. 16 is obviously only an estimate of the physical situation which, in reality, involves local anisotropy, crystallographic features, roughness, etc. The trend, however, matches very well with the observed experimental behaviour and the estimate of a saturation or transition length, c_1, to conventional LEFM behaviour is expected. It is also shown to be correct since this is the length which defines the boundary beyond which an overall continuum treatment involving self-similarity is permissible.

Summary and conclusions

This investigation was carried out to provide a comparison of the high-cycle fatigue properties, the initiation, and growth of microstructurally short to long

fatigue cracks, and the threshold behaviour at various stress ratios for two technical high strength Al alloys, Al 2024-T3 and Al 7475-T6. The test results and the conclusions from this study can be summarized as follows.

(1) The *S–N* data indicate that for symmetrical loading the fatigue limit is not reached prior to $N = 10^8$ in both alloys. The effect of specimen orientation (L or T) on the fatigue limit is minor; the stronger alloy 7475 exhibits a higher fatigue limit than alloy 2024.

(2) Long-crack threshold stress intensity values depend on the applied stress ratio (in the range $-1 \leq R \leq 0.75$). In contrast, the effective threshold stress intensities appear to fall within a single scatter band. The effect of specimen orientation on threshold is particularly noticable for R values near zero. For the alloy 7475 both long-crack threshold values fall below those of alloy 2024.

(3) In tests carried out near the fatigue limit the initiation of microcracks was observed to occur in alloy 2024 at bulky intermetallic particles cracked during cyclic loading, while in alloy 7475 crack initiation was observed either at the particle/matrix interface or along slip lines present in the as-received microstructure. The initially transcrystalline microcracks were invariably oriented at an angle of approximately 45 degrees to the stress axis.

(4) Threshold stresses for microcracks growing within a single grain were observed, but only at very small loading amplitudes.

(5) Microcracks up to a characteristic critical length were observed to grow only at stress amplitudes at, or slightly above, the fatigue limit. Retardation or halts of the advancing crack tips occurred predominantly by interaction with grain boundaries; at low stress amplitudes cracks were found to remain halted for 10^7 cycles. Slight increases in stress amplitude caused a resumption of the crack advance, accelerating after traversing the blocking grain boundary and decelerating again at the approach of the next grain boundary. The extent of retardation and the maximum growth rate between these interactions depended sensitively on cyclic amplitude and stress ratio. The number of repetitions of this interaction sequence was related to the grain dimensions in the crack growth direction.

(6) The anomalies typical for short fatigue cracks extended up to a characteristic transition length which was found to depend on the alloy but not on grain dimensions or specimen orientation. Up to this transition length short-crack growth occurred only at, or slightly above, the fatigue limit; the growth behaviour of these short cracks cannot be described by LEFM terms. Cracks beyond this length were found to resume growth at stress levels progressively lowered with increasing crack length, until crack growth took place at stress levels corresponding to the threshold stress intensity of long cracks. Thus, the transition length approximates the limit for true short-crack growth behaviour.

(7) The transition length can be calculated from the effective threshold stress intensity value and the stress level corresponding to the fatigue limit. This fact clearly indicates the governing role of closure in the short crack behaviour. It is interesting to note that the transition length is much shorter for alloy 7475 than for alloy 2024.

(8) The transition length can also be deduced from corroborating observations of changes in the fracture path topography with increasing crack length, i.e., from crystallographic stage I (single crack plane through entire grains) to crystallographic stage II (transcrystalline crystallographic zigzagging along a line normal to the stress axis). The final transition to non-crystallographic stage II indicates the crack length for which conventional LEFM-considerations are applicable.

(9) A Kitagawa-type diagram reveals the influence of differences in fatigue strength and long-crack threshold values. The limiting length for short-crack behaviour is uniquely defined by the line corresponding to the effective stress intensity of long cracks. To demonstrate the effects of varying stress ratios, plotting of the test results in a modified diagram with the maximum stress rather than the stress range as abscissa is suggested. In this way the anticipated reduction of transition length with increasing stress ratio is revealed by the intersections with the line corresponding to the effective threshold stress intensity.

(10) The experimental and computational results of this investigation imply that, for design considerations, the LEFM relations can be applied to small fatigue cracks exceeding the transition length (in the order of 150 μm in high-strength Al alloys) if the effective threshold values for long cracks are taken into account. In his way uncertainties caused by varying stress ratios are eliminated. Further investigations, however, are required to understand the true short-crack growth mechanism, which appears to be of rather academic interest because it concerns crack lengths below engineering detectability.

Acknowledgements

The investigations were partly supported by the Swedish Board for Technical Development, by the Fonds zur Förderung der wissenschaftlichen Forschung, and by the Hochschuljubiläumsstiftung der Stadt Wien, Austria. The authors thank Dr A. Hadrboletz for calibration measurements.

References

(1) de LANGE, R. G. (1964) Plastic replica methods applied to a study of fatigue crack propagation, *Trans. AIME*, **230**, 644–648.
(2) PEARSON, S. (1975) Investigation of fatigue cracks in commercial Al alloys and subsequent propagation of very short fatigue cracks, *Engng Fracture Mech.*, 7, 235–247.
(3) SCHIJVE, J. (1984) The practical and theoretical significance of small cracks. An evaluation, *Fatigue 84* (EMAS, Warley), p. 751.

(4) JEAL, R. H. (1985) The specification of gas turbine disc forgings, *Metals Mater.*, **1**, 528–533.
(5) NISITANI, H. and TAKAO, K. I. (1981) Significance of initiation, propagation, and closure of microcracks in HCF of ductile materials, *Engng Fracture Mech.*, **15**, 445–456.
(6) MILLER, K. J. (1982) The short crack problem, *Fatigue Engng Mater. Structures*, **5**, 223–232.
(7) RITCHIE, R. O. and SURESH, S. (1982) Mechanics and physics of the growth of small cracks, Proc. AGARD 55th SMP meeting, Toronto.
(8) RITCHIE, R. O. (1983) Fracture mechanics approach to fatigue crack propagation, *Encyclopedia of Materials Science and Engineering* (Pergamon Press, Oxford).
(9) MILLER, K. J. (1984) Initiation and growth rates of short fatigue cracks. *Eshelby Memorial Conference* (*IUTAM*) (Cambridge University Press), pp. 477–500.
(10) SURESH, S. and RITCHIE, R. O. (1984) Propagation of short fatigue cracks, *Int. Met. Rev.*, **29**, 445–476.
(11) PINEAU, A. (1984) Short fatigue cracks and crack closure, *Proc. ECF-5*.
(12) TAYLOR, D. (1982) EUROMECH 151 colloquium on short fatigue cracks, *Fatigue Engng Mater. Structures*, **5**, 305–309.
(13) JAMES, M. R., MORRIS, W. L., and ZUREK, A. K. (1983) On the transition from near-threshold to intermediate growth rates in fatigue, *Fatigue Engng Mater. Structures*, **6**, 293–305.
(14) FATHULLA, A., WEISS, B., STICKLER, R., and FEMBÖCK, J. (1985) The initiation and growth of short cracks in pm-Mo and Mo-alloys, proc. 11th Int. Plansee Seminar, paper RM 11, p. 45.
(15) MORRIS, W. L. (1977) The early stages of fatigue crack propagation in Al 2048-T851, *Met. Trans*, **8A**, 589–596.
(16) FATHULLA, A., WEISS, B., and STICKLER, R. (1984) Initiation and propagation of short cracks under cyclic loading near threshold in technical alloys, Proc. Spring Meeting French Metals Society, Paris, p. 182.
(17) FATHULLA, A., WEISS, B., and STICKLER, R. (1984) Initiation and propagation of short cracks under cyclic loading of Al 2024 near threshold, *Fatigue 84* (EMAS, Warley), p. 1913.
(18) FOTH, J., MARISSEN, R., NOWACK, H., and LÜTJERING, G. (1984) Fatigue crack initiation and microcrack propagation in notched and unnotched Al 2024-T3 specimens, Proc. ICAS 1984, p. 791.
(19) KUNG, C. Y. and FINE, M. E. (1979) Fatigue crack initiation and microcrack growth in Al 2024-T4 and 2124-T4 Al alloys, *Met. Trans*, **10A**, 603–610.
(20) MORRIS, W. L. and BUCK, O. (1977) Crack closure load measurements for microcracks developed during fatigue of Al 2219-T851, *Met. Trans*, **8A**, 597–601.
(21) MORRIS, W. L. (1977) Crack closure load development for surface microcracks in Al 2219-T851, *Met. Trans*, **8A**, 1079–1086.
(22) MORRIS, W. L. (1977) A comparison of microcrack closure load development for stage I and II cracking events for Al 7075-T651, *Met. Trans*, **8A**, 1087–1093.
(23) MORRIS, W. L. (1979) Microcrack closure phenomena for Al 2219-T851, *Met. Trans*, **10A**, 5–11.
(24) JAMES, M. R. and MORRIS, W. L. (1983) Effect of fracture surface roughness on growth of short fatigue cracks, *Met. Trans*, **14A**, 153–155.
(25) TAYLOR, D. and KNOTT, J. F. (1981) Fatigue crack propagation behaviour of short cracks, the effect of microstructure, *Fatigue Engng Mater. Structures*, **4**, 147–155.
(26) MORRIS, W. L. and JAMES, M. R. (1984) Investigation of the growth threshold for short cracks, Proc. Fat. Thresholds, Philadelphia, p. 479.
(27) SURESH, S. (1983) Crack deflection: implication for the growth of long and short fatigue cracks, *Met. Trans*, **14A**, 2375–2385.
(28) SURESH, S. (1985) Fatigue crack deflection and fracture surface contact: micromechanical models, *Met. Trans*, **16A**, 249–260.
(29) LANKFORD, J. (1985) The influence of microstructure on the growth of small fatigue cracks, *Fatigue Fracture Engng Mater. Structures*, **8**, 161–175.
(30) HIROSE, S. and FINE, M. E. (1983) Fatigue crack initiation and microcrack propagation in X7091 type Al p/m alloys, *Met. Trans*, **14A**, 1189–1197.
(31) ALLEN, R. J. and SINCLAIR, J. C. (1982) The behavior of short cracks. *Fatigue Engng Mater. Structures*, **5**, 343–347.

(32) BLOM, A. F. and HOLM, D. K. (1985) An experimental and numerical study of crack closure, *Engng Fracture Mech.*, **22**, 997–1011.
(33) TANAKA, K. NAKAI, Y., and YAMASHITA, M. (1981) Fatigue growth threshold of small cracks, *Int. J. Fracture*, **17**, 519–533.
(34) NEWMAN, J. C. (1982) A non-linear FM approach to the growth of small cracks, Proc. AGARD 55th SMP meeting, Toronto.
(35) HOBSON, P. D. (1982) The formulation of a crack growth equation for short cracks, *Fatigue Engng Mater. Structures*, **5**, 323–327.
(36) COOPER, C. V. and FINE, M. E. (1984) Coffin–Manson relationship for fatigue crack initiation, *Scripta Met.*, **18**, 593–596.
(37) DE LOS RIOS, E. R., MOHAMED, H. J. and MILLER, K. J. (1985) A micro-mechanics analysis for short fatigue crack growth, *Fatigue Fracture Engng Mater. Structures*, **8**, 49–63.
(38) KITAGAWA, H. and TAKAHASHI, S. (1976) Applicability of fracture mechanics to very small cracks or the cracks in the early stages, Proc. ICM-2, ASM, p. 627.
(39) USAMI, S. and SHIDA, S. (1979) Elastic–plastic analysis of the fatigue limit for a material with small flaws, *Fatigue Engng Mater. Structures*, **1**, 471–481.
(40) MORRIS, W. L., JAMES, M. R. and BUCK, O. (1981) Growth rate models for short surface cracks in Al 2219-T851, *Met. Trans*, **12A**, 57–64.
(41) MORRIS, W. L., JAMES, M. R., and ZUREK, A. K. (1985) The extent of crack tip plasticity for short fatigue cracks, *Scripta Met.*, **19**, 149–153.
(42) ZUREK, A. K., JAMES, M. R., and MORRIS, W. L. (1983) The effect of grain size on the fatigue crack growth of short cracks, *Met. Trans*, **14A**, 1697–1705.
(43) TAYLOR, D. (1984) The effect of crack length on fatigue threshold, *Fatigue Engng Mater. Structures*, **7**, 267–277.
(44) LANKFORD, J. (1982) The growth of small fatigue cracks in 7075-T6 Al, *Fatigue Engng Mater. Structures*, **5**, 233–248.
(45) CHAN, K. S. and LANKFORD, J. (1983) A crack tip strain model for growth of small fatigue cracks, *Scripta Met.*, **17**, 529–532.
(46) LANKFORD, J. and DAVIDSON, D. L. (1983) Near threshold crack tip strain and crack opening for large and small fatigue cracks, Proc. Threshold Conf., Philadelphia.
(47) CHANANI, G. R., TELESMAN, I., BRETZ, P. E., and SCARICH, G. V. (1982) Methodology for the evaluation of fatigue crack growth resistance of Al alloys, Northrop Corporation Technical Report.
(48) STICKLER, R. and WEISS, B. (1982) Review of the application of ultrasonic fatigue test methods for the determination of crack growth and threshold behavior of metallic materials, *Proc. Int. Conf. on ultrasonic fatigue* (Edited by J. Wells) (AIME), p. 135.
(49) ASTM working document E647 – *Standard test method for measurement of fatigue crack growth rates*, 1985.
(50) BLOM, A. F., HADRBOLETZ, A., and WEISS, B. (1983) Effect of crack closure on near-threshold crack growth behavior in a high-strength Al-alloy up to ultrasonic frequencies, *Proc. ICM-4*.
(51) ASTM E740-80 – *Standard practice for fracture testing with surface crack tension specimens*, ASTM 1983-3-03.01).
(52) BLOM, A. F., HADRBOLETZ, A. and WEISS, B. unpublished results.
(53) LUKAS, P., KUNZ, L., KNESL, Z., WEISS, B., and STICKLER, R. (1985) Fatigue crack propagation rate and the crack tip plastic strain amplitude in polycrystalline Cu, *Mater. Sci. Engng*, **70**, 91–100.
(54) WEISS, B., MÜLLNER, H., STICKLER, R. LUKAS, P., and KUNZ, L. (1984) Influence of frequency on fatigue limit and fatigue crack growth behaviour of polycrystalline Cu, *Proc. ICF-6*, Vol. 3, p. 1783.
(55) ZAIKEN, E. and RITCHIE, R. O. (1985) On the development of crack closure and the threshold condition for short and long fatigue cracks in Al 7150, *Met. Trans*, **16A**, 1467–1477.
(56) HOLM, D. K. and BLOM, A. F. (1984) Short cracks and crack closure in Al 2024-T3, *Proc. ICAS* (ICAS-84-3.7.1), p. 783.